



Efficient Part Recognition Method in Vision Guided Robots using Orthogonal Moments

Bunil Kumar Balabantaray^{1*}, Rabindra Narayan Mahapatra², Bibhuti Bhusan Biswal³

¹Assistant Professor, Department of Computer Science and Engineering

²Associate Professor, Department of Mechanical Engineering

³Professor and Director, Senior Member IEEE, Department of Mechanical Engineering

^{1,2,3}National Institute of Technology Meghalaya INDIA

*Corresponding author E-mail: bunil@nitm.ac.in

Abstract

The best method in developing automated assembly system is the integration of the machine vision tools with the robot in the assembly platform. Vision system plays an important role in building an autonomous robotic part assembly system. Recognition of the correct part in the assembly line is the key issue while grasping the parts by the robot. The captured images of the parts on the assembly line may be affected by geometric transformation such as rotation, translation, scaling and may be corrupted by Point-Spread-Function (PSF) blurring of camera. In order to recognize parts in such type of condition, three steps are followed in this paper. Firstly, features of the parts are extracted by using combined orthogonal Zernike moment. Secondly, the original part image is reconstructed by using combined orthogonal Zernike moment. For this reconstruction, the moment order is selected by a proposed algorithm. The optimum moment order will maintain a proper balance between the reconstruction capability and sensitivity to noise. Finally, for classification of parts used in assembly nearest-neighbor classifier is used. The suggested technique is implemented in LabVIEW and the simulation is successfully performed in an assembly system with 6-DoF Kawasaki robot.

Keywords: Object classification; Zernike moment; Nearest-neighbor; Vision guided robot.

1. Introduction

The parts in the assembly lines are transported to the assembly station by means of material handling devices. The captured images of the parts on the assembly station belt may be affected by transformation with respect to geometry of the object/parts such as scaling, translation, rotation and may be corrupted by Point-Spread-Function (PSF) blurring of camera. The proposed method utilizes orthogonal moment based feature attributes for object recognition. These attributes are insensitive to geometric transformation and blurring conditions present in the acquired images. Moreover, the environmental noise which is inherently present in the captured images, is taken care in this method.

Object recognition is a very important and necessary image processing step in the arena of machine vision. Popularly, the object recognition procedure follows four subsequent steps such as

- Image acquisition
- Image preprocessing
- Feature extraction
- Classification

Feature extraction is the most vital and principal activity in the field of object recognition. It is due to the fact that the features have the ability to represent an image via some distinctive and characteristic interest points. Consequently this process reduces the amount of data required to represent an object. Recognition of objects irrespective of their position, size, and geometrical trans-

formation has been an active research area from last decades. The key solution to this type of problem lies in selecting object descriptors which are invariant in nature. However, whatever may be the type of object descriptors, they should take care of some of the main issues as described below.

- Selection of a feature descriptor which is invariant to image position, scale and orientation.
- Selection of a feature descriptor which is robust to noise or any other degradation present in the imagery.
- Selection of a feature descriptor which can represent the object or image compactly.
- Selected feature descriptor must maintain a tradeoff between the time and space efficiency.

2. Background

Among a variety of alternatives, object recognition via moment invariants [M. K. Hu 1962; J. Flusser, 2006; Mercimek et al., 2005], and Fourier descriptor are quite prominent in literature. Among all of the above mentioned object descriptors, moment invariants are extensively used in object recognition as they satisfy almost all these requirements of a good object descriptor [Khotanzad et al., 1990]. Therefore, this work focuses on the moment invariants to provide a suitable background for object identification.

Moment invariants are those features of the image which retain their values when the image undergoes different degradations such as shift, scaled, or rotation and blur. Moment invariants are calculated in terms of ordinary moments. Due to this excellent behavior, moment invariants have been widely used in numerous applications such as object recognition, image classification [Keyes et al., 2001], template matching [K. M. Hosny, 2010] and image registration [Flusser et al., 1994] etc.

3. Methodology

The invariant features of the image are used as the input to the classification process to select the labeling of the underlying image. Hence, extraction of appropriate feature attributes is so much important in the process of object identification. However, along with the extraction of feature attributes some other factor such as deciding the optimal number of feature vector which can represent the image compactly as well what is the amount of contribution of each feature vector towards the image representation also impact on the success of the method. The majority of the existing states of art techniques in literature use an unplanned procedure for achieving such requirements. Furthermore, from the indigenous study of object identification in literature it is observed for the identification of a blurred image is performed by de-blurring that image prior to apply the image identification methods. However, de-blurring of an image without the prior knowledge about the blurring parameter is ill-posed in nature and till now it is also an open research area.

In order to take care of the above mentioned issues, the proposed work aims at utilizing a set of feature attributes of the captured images that are invariant to geometric transformations such as scaling, translation and rotation as well as to blurring environments. They are the feature attributes which are invariant to similarity transformation and blur by using orthogonal Zernike moments (ZM) [Khotanzad et al., 1990]. Besides this, a systematic reconstruction based approach is used for the selection of optimal order of the orthogonal ZM required in the classification problem is established.

The reason why to use orthogonal Zernike moments:

- Noise sensitivity of ZM are better than other types of moments
- ZM outperform non-orthogonal and other orthogonal moments in terms of providing redundant information and image representation competence.

The rest of the discussion follows the sequence of procedures followed for the object recognition.

3.1 Mathematical Background of Zernike Moment

ZM of order n with recurrence l to intensity of image $f(x, y)$ is given [Chong et al., 2004] in Eq. 1

$$\square_{nl} = \frac{n+1}{\pi} \sum_x \sum_y R_{nl}(\rho) \exp(jl\theta) f(x, y) dx dy \quad (1)$$

$$n \geq 0, |l| \leq n, n - |l| \text{ is even.}$$

Where $R_{nl}(\rho)$ describes the real valued radial polynomial and is described in Eq.1

$$R_{nl}(\rho) = \sum_{s=0}^{\frac{n-|l|}{2}} (-1)^s \frac{(n-s)!}{s! \left(\frac{n+|l|}{2} - s\right)! \left(\frac{n-|l|}{2} - s\right)!} \rho^{n-2s} \quad (2)$$

In order to compute the ZM of an image the first and foremost step is to map the center of the image into origin and to map all of

the pixel coordinates to arrange of unit circle $(x^2 + y^2)$. The pixels within that unit circle contribute in the computation of ZM whereas the pixels outside the unit circle don't contribute. Imperfect mapping scheme will introduce geometric error in the computation of ZM. Hence in order to avoid geometric error the proposed work utilizes the mapping scheme as given in [Yang et al., 2010] and is described in Eq. 3.

$$\{f(x, y)\}_{M \times M} \rightarrow \{f(u_i, v_j)\}_{[-1,1] \times [-1,1]} \quad (3)$$

$$\text{Where, } u_i = a \left(i + \frac{1}{2} \right) + b \quad i = 0, 1, \dots, (M-1)$$

$$v_j = a \left(j + \frac{1}{2} \right) + b \quad j = 0, 1, \dots, (M-1)$$

$$a = \frac{2c}{M-1}; b = -c; c = \frac{1}{\sqrt{2}}$$

The intensity image $f(x, y)$ of size $(M \times N)$ is mapped to $f(u_i, v_j)$ onto the unit circle.

3.2 Formation of Feature Attributes

This section describes the process of generating a set of feature attributes based on combined orthogonal ZM invariants. These attributes are not only invariant to geometric transformation such as rotation, scaling, translation but also insensitive to the blurring conditions [Chen et al. 2011]. The combined orthogonal ZM invariant order n with recurrence l for $f(x, y)$ is denoted as $CI(n, l)^{f(x, y)}$. Eq. 4 provides the mathematical formulation for $CI(n, l)^{f(x, y)}$ at $n-l+2p$.

$$CI(l+2p, l)^{f(x, y)} = e^{-jl\theta_f} \sum_{m=0}^p \sum_{k=0}^p \Gamma_{f(x, y)}^{-(l+2k+2)} C_{p, k}^l D_{k, m}^l I(l+2m, l)^{f(x, y)} \quad (4)$$

Where $\Gamma_{f(x, y)} = \sqrt{\square_{00}}$ and $\theta_f = \arg(\square_{11})$. \square_{nl} defines the ZM of digital image of order n with l repetition and is defined in Eq. 1. The formulation of $C_{p, k}^l$ and $D_{k, m}^l$ is described in Eq.

5 and Eq. 6 respectively. $I(l+2p, l)^{f(x, y)}$ is the set of feature attributes based on ZM invariant to blurring condition and is described in Eq. 7.

$$C_{p, k}^l = (-1)^{p-k} \frac{l+2p+1}{\pi} \frac{(l+p+k)!}{k!(p-k)!(l+k)!} \quad (5)$$

$$D_{k, m}^l = \frac{k!(l+k)! \pi}{(k-m)!(l+k+m+1)!} \quad (6)$$

$$I(l+2p, l)^{f(x, y)} = \square_{l+2p, l} - \frac{1}{\square_{00\pi}} \sum_{t=0}^{p-1} I(l+2t, l)^{f(x, y)} \sum_{j=1}^{p-1} \square_{2j, 0} A(l, p, t, j) \quad (7)$$

Where the formulation for $A(l, p, t, j)$ is described in Eq. 8

$$A(l, p, t, j) = \sum_{k=t+j}^p \sum_{n=t}^{k-j} \binom{l+k}{l+n} \binom{k}{n} C_{p,k}^l D_{n,t}^l D_{k-n,j}^0 \quad (8)$$

3.3 Image Reconstruction using Combined Orthogonal Moment

This section describes the reconstruction of a digital image $f(x, y)$ by utilizing the feature attributes up to a predefined order o_{\max} based on combined invariant to similarity transformation and to blur using orthogonal ZM of the captured image $f(x, y)$. Eq. 9 provides the mathematical formulation for

the estimation of $f(x, y)$.

$$f(x, y) = \sum_{k=0}^{o_{\max}} \sum_{l=k+2p}^{o_{\max}} CI(l+2p, l) f^{(x,y)} R_{kl}(\rho) \exp(jl\theta) \quad (9)$$

When $o_{\max} \rightarrow \infty$, then the $f(x, y)$ will approach towards $f(x, y)$. However, it is quite difficult to find out the optimal value of o_{\max} i.e., o_{opt} for which the reconstructed image

$f(x, y)$ approaches to the true estimate $f(x, y)$. From the literature it is quite obvious that as the moment order increases the noise sensitivity also increase. Moment invariants of lower order are less sensitive to noise but have limited representation capability. Hence, a strategy is proposed to select the optimal order, o_{opt} , which will maintain a trade-off between the reconstruction capability and noise sensitivity.

3.4 Selection of Optimal Moment Order (o_{opt})

This discussion provides the way to choose the optimum moment order of the combined invariants for which $f(x, y)$ will approach towards $f(x, y)$ and the reconstruction process should be less affected by noise. Algorithm 1 describes the optimization process utilized for the selection of optimal order o_{opt} . The cost function of the optimization process is to minimize the inter-correlation gap between the captured and estimated image. However, correlation between the captured and estimated image is modeled as an energy function.

Algorithm 1:

Selection of optimal moment order o_{opt}

Input: $f(x, y)$, $f(x, y)$, o_{\max} and

Output: o_{opt}

Step 1: For $i=2$ to o_{\max} do

Step 2: Find the amount of correlation between the image $f(x, y)$ and $f(x, y)$ by using the following equation

$$corr(i) = \frac{\sum_m \sum_m \left(\hat{f}^i(x,y) - \text{mean}(\hat{f}^i(x,y)) \right) \left(f(x,y) - \text{mean}(f(x,y)) \right)}{\sqrt{\left(\sum_M \sum_M \left(\hat{f}^i(x,y) - \text{mean}(\hat{f}^i(x,y)) \right)^2 \right) \left(\sum_M \sum_M \left(f(x,y) - \text{mean}(f(x,y)) \right)^2 \right)}} \quad 0 \leq corr(i) \leq 1$$

Step 3: If $(corr(i) \geq \varepsilon)$ $0 \leq \varepsilon \leq 1$ then $i = o_{opt}$

That means with the current moment order i the correlation between the captured and original image is quite high and no more improvement is needed in the reconstruction process.

Else go to step 4

Step 4: Perform minimization of the energy function as

described in the following equation to find o_{opt}

$$o_{opt} = \arg \min_{o_{opt}} \sum_{x=1}^M \sum_{y=1}^M \left(f(x, y) - f^{o_{\max}}(x, y) \right)^2$$

The above equation measures the grid point gap. By considering the mapping scheme as described in Eq. 3, the empirical solution to the above minimization problem is given below.

$$o_{opt} = \Delta x \Delta y \sum_{x=1}^M \sum_{y=1}^M \left(f(x, y) - f^{o_{\max}}(x, y) \right)^2 \gamma(o_{opt})$$

where $(\Delta x, \Delta y)$ defines the pixel interval in the mapping process. $\gamma(o_{opt})$ denotes the penalty factor and is defined as

$$\gamma(o_{opt}) = \left(1 - \left(\frac{(o_{\max} + 1)(o_{\max} - 1)}{2} \right) \Delta x \Delta y \right)^{-1}$$

Step 5: end For

Step 6: Obtain the optimum moment order o_{opt} .

The accuracy of the o_{opt} resulted by Algorithm 1 is verified by experimental analysis. In the experimental analysis, the plot of normalized reconstruction error for the reconstruction of $f(x, y)$ using the combined moment invariants $CI(l+2p, l)^{f(x,y)}$ of order zero through $o_{\max} = 15$ from the captured image $f(x, y)$ is plotted in Fig. 1. The plot is the average plot for the 4 test part images such as "Part1.jpg", "Part2.jpg", "Part3.jpg" and "Part 4" as shown in Fig.2 to fig. 5. The reconstruction error is computed using Eq. 10. From the plot it is clearly visible that with the increase in moment order the reconstruction error reduces gradually. The minimal error is found approximately at 6th order. After that the reconstruction error starts increasing. Hence, the o_{opt} from the experimental study is found to be at 6th order and is termed as $\{o_{opt}\}_{Ex}$. However, the selection of o_{opt} by using Algorithm 1 is found to be 7 and is termed as $\{o_{opt}\}_{Al}$. The relative error between the selections of optimum order moment can be determined by the formulation given in Eq. 11 and is found to be 3.32%.

$$error^2 = \frac{\sum_{x=0}^{M-1} \sum_{y=0}^{M-1} \left(f(x, y) - f(x, y)^{o_{max}} \right)^2}{\sum_{x=0}^{M-1} \sum_{y=0}^{M-1} (f(x, y))^2} \quad (10)$$

$$relativeerror \left(\{o_{opt}\}_{Ex} \{o_{opt}\}_{Al} \right) = \frac{\left\| \begin{matrix} \{o_{opt}\}_{Al} & \{o_{opt}\}_{Ex} \\ f(x, y) - f(x, y) \end{matrix} \right\|}{\left\| \begin{matrix} \{o_{opt}\}_{Al} \\ f(x, y) \end{matrix} \right\|} \quad (11)$$

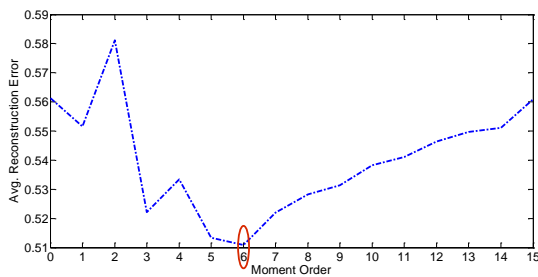


Fig.1: Average reconstruction error vs Moment order

4. Result Analysis for the Invariance Measure

Simulation results demonstrate the efficacy and robustness of the proposed method. Tests are performed in two different scenarios. The first experiment is tested with different synthetically generated test images and the second experiment is tested on the real images captured from the conveyor belt. To test the invariance of moment invariants towards the geometrical transformation and to blurring condition, test images are generated synthetically for four parts such as “part1.jpg”, “part2.jpg”, “part3.jpg”, and “part4.jpg”. The synthetic images are rotated by different angles from $\theta = 5^\circ$ to 150° and different scaling parameters as well as three different types of blurring kernels are also used. The parameters used for creating synthetic images are Δx , Δy , θ and S . Δx and Δy represent the translation along X-axis and Y-axis respectively. θ and S defines the angle of rotation and amount of scaling respectively. The blurring types such as average blur with size (7 x7), Gaussian blur with size (31 x 31) with standard deviation=0.1 and motion blur with parameter (20,45) are used. The detail description about the parameters used for generating the synthetic images for different sample part images are given in Table 1. Fig. 2 to Fig. 5 provides the graphical representation of the synthetically generated images.

Table 1: Parameters used for creating synthetic images

(a) Original image	(b) Average Blur (7x7)	(c) Gaussian Blur (31x31)	(d) Motion Blur (20,45)
Part1.jpg	$\Delta x = -5,$ $\Delta y = 7,$ $\theta = 30,$ $S = 0.5$	$\Delta x = -5,$ $\Delta y = 5,$ $\theta = 150,$ $S = 0.75$	$\Delta x = -1,$ $\Delta y = 6,$ $\theta = 60,$ $S = 1$
Part2.jpg	$\Delta x = -5,$ $\Delta y = 7,$ $\theta = 30,$ $S = 0.5$	$\Delta x = -5,$ $\Delta y = 5,$ $\theta = 150,$ $S = 0.75$	$\Delta x = -1,$ $\Delta y = 6,$ $\theta = 60,$ $S = 1$
Part3.jpg	$\Delta x = -5,$ $\Delta y = 7,$	$\Delta x = -5,$ $\Delta y = 5,$	$\Delta x = -1,$ $\Delta y = 6,$

	$\theta = 30,$ $S = 0.5$	$\theta = 150,$ $S = 0.75$	$\theta = 60,$ $S = 1$
Part4.jpg	$\Delta x = -5,$ $\Delta y = 7,$ $\theta = 30,$ $S = 0.5$	$\Delta x = -5,$ $\Delta y = 5,$ $\theta = 150,$ $S = 0.75$	$\Delta x = -1,$ $\Delta y = 6,$ $\theta = 60,$ $S = 1$

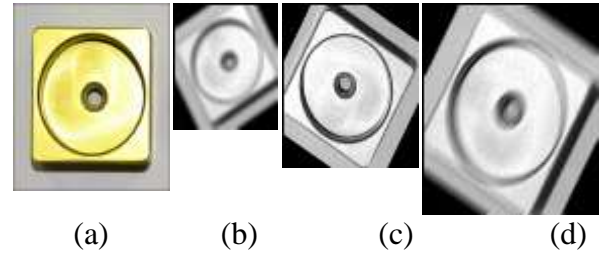


Fig. 2: Synthetically generated images for original image “Part1.jpg”

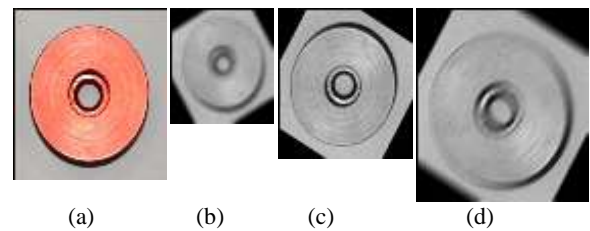


Fig. 3: Synthetically generated images for original image “Part2.jpg”

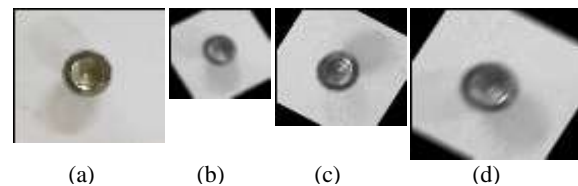


Fig. 4: Synthetically generated images for original image “Part3.jpg”

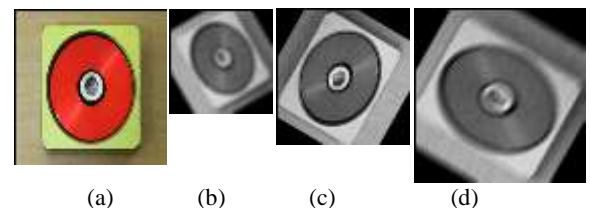


Fig. 5: Synthetically generated images for original image “Part4.jpg”

The invariants values of different order up to order for the synthesized images are given in Table 1 through Table 5. By analyzing the data given in the tables, it is observed that, there exist excellent invariance measures among the test images regardless of the image degradation. Consequently, the proposed method recognizes the parts efficiently in the conveyor belt.

Table 1: Combined moment invariant (order 6) for synthetic images of “Part1 .jpg” image

Moment invariants	Fig. 2(a)	Fig. 2(b)	Fig. 2 (c)	Fig. 2(d)
CI(2,0)	5.57e-02	5.57e-02	5.58e-02	5.57e-02
CI(2,2)	2.33e-03	2.33e-03	2.33e-03	2.30e-03
CI(3,1)	3.61e-04	3.61e-04	3.61e-04	3.60e-04
CI(3,3)	5.97e-04	5.97e-04	5.96e-04	5.98e-04
CI(4,0)	4.39e-03	4.39e-03	4.40e-03	4.42e-03
CI(4,2)	3.31e-02	3.31e-02	3.31e-02	3.31e-02
CI(4,4)	4.55e-05	4.55e-05	4.55e-05	4.55e-05
CI(5,1)	2.00e-02	2.00e-02	2.00e-02	2.00e-02
CI(5,3)	2.66e-02	2.66e-02	2.64e-02	2.66e-02
CI(5,5)	5.23e-05	5.23e-05	5.23e-05	5.20e-05
CI(6,0)	1.32e-04	1.32e-04	1.32e-04	1.32e-04
CI(6,2)	2.54e-06	2.54e-06	2.54e-06	2.54e-06

CI(6,4)	3.11e-05	3.10e-05	3.11e-05	3.11e-05
CI(6,6)	6.55e-06	6.55e-06	6.55e-06	6.55e-06

Table 2: Combined moment invariant (order 6) for synthetic images of "Part2.jpg" image

Moment invariants	Fig. 3(a)	Fig. 3 (b)	Fig. 3 (c)	Fig. 3 (d)
CI(2,0)	1.54e-02	1.54e-02	1.54e-02	1.54e-02
CI(2,2)	4.65e-03	4.66e-03	4.65e-03	4.65e-03
CI(3,1)	4.55e-04	4.55e-04	4.55e-04	4.55e-04
CI(3,3)	6.40e-04	6.41e-04	6.40e-04	6.40e-04
CI(4,0)	5.87e-03	5.87e-03	5.87e-03	5.87e-03
CI(4,2)	3.23e-02	3.23e-02	3.21e-02	3.23e-02
CI(4,4)	5.12e-05	5.12e-05	5.12e-05	5.12e-05
CI(5,1)	2.79e-02	2.79e-02	2.79e-02	2.80e-02
CI(5,3)	3.07e-02	3.07e-02	3.07e-02	3.06e-02
CI(5,5)	4.10e-05	4.10e-05	4.11e-05	4.10e-05
CI(6,0)	3.78e-04	3.78e-04	3.78e-04	3.78e-04
CI(6,2)	4.10e-06	4.10e-06	4.11e-06	4.10e-06
CI(6,4)	4.44e-05	4.44e-05	4.42e-05	4.43e-05
CI(6,6)	7.80e-06	7.80e-06	7.79e-06	7.82e-06

Table 3: Combined moment invariant (order 6) for synthetic images of "Part3.jpg" image

Moment invariants	Fig. 4(a)	Fig. 4 (b)	Fig. 4 (c)	Fig. 4 (d)
CI(2,0)	3.16e-03	3.16e-03	3.16e-03	3.16e-03
CI(2,2)	5.48e-04	5.48e-04	5.48e-04	5.47e-04
CI(3,1)	5.70e-05	5.70e-05	5.70e-05	5.70e-05
CI(3,3)	2.13e-05	2.13e-05	2.13e-05	2.13e-05
CI(4,0)	5.17e-04	5.17e-04	5.17e-04	5.15e-04
CI(4,2)	2.46e-03	2.46e-03	2.46e-03	2.47e-03
CI(4,4)	3.57e-06	3.57e-06	3.55e-06	3.57e-06
CI(5,1)	3.88e-03	3.88e-03	3.89e-03	3.88e-03
CI(5,3)	4.30e-03	4.31e-03	4.30e-03	4.30e-03
CI(5,5)	5.37e-06	5.37e-06	5.37e-06	5.35e-06
CI(6,0)	4.66e-05	4.66e-05	4.64e-05	4.66e-05
CI(6,2)	3.23e-07	3.23e-07	3.22e-07	3.23e-07
CI(6,4)	4.48e-06	4.48e-06	4.48e-06	4.49e-06
CI(6,6)	5.56e-07	5.56e-07	5.56e-07	5.56e-07

Table 4: Combined moment invariant (order 6) for synthetic images of "Part4.jpg" image

Moment invariants	Fig.5(a)	Fig. 5(b)	Fig.5 (c)	Fig.5(d)
CI(2,0)	2.13e-02	2.13e-02	2.13e-02	2.13e-02
CI(2,2)	4.33e-04	4.33e-04	4.33e-04	4.34e-04
CI(3,1)	5.18e-05	5.18e-05	5.18e-05	5.18e-05
CI(3,3)	3.16e-06	3.16e-06	3.17e-06	3.18e-06
CI(4,0)	4.44e-04	4.44e-04	4.44e-04	4.44e-04
CI(4,2)	6.37e-03	6.38e-03	6.38e-03	6.37e-03
CI(4,4)	4.42e-05	4.42e-05	4.42e-05	4.41e-05
CI(5,1)	3.90e-04	3.92e-04	3.91e-04	3.90e-04
CI(5,3)	3.32e-03	3.32e-03	3.32e-03	3.32e-03
CI(5,5)	5.46e-05	5.46e-05	5.46e-05	5.44e-05
CI(6,0)	2.23e-04	2.22e-04	2.20e-04	2.21e-04
CI(6,2)	1.12e-06	1.10e-06	1.12e-06	1.12e-06
CI(6,4)	4.05e-05	4.05e-05	4.05e-05	4.05e-05
CI(6,6)	4.58e-06	4.51e-06	4.56e-06	4.58e-06

4.1 Object Classification using Nearest-Neighbor Method

In this step the classification of an image is done by passing the k-dimensional optimal feature attributes to a nearest-neighbor (NN) classifier. The optimal feature attributes are obtained from the utilized combined invariants $CI(l+2p,l)^f(x,y)$ of order $o_{opt} = 6$. With this moment order, the images can be appropriately represented by only 14 number of feature attributes. As a result, the computational burden of the whole system will reduce to a larger extent.

Fig. 6 shows the block diagram for the above process. The main aim of the image classification is to label an unknown image I into a class c provided a database of N classified images. For which, we have first find out the 14 optimal feature attributes (using the feature attributes with $o_{opt} = 6$) of image. Next step is to find out the 14 optimal feature attributes for each of the classified images present in the database. Image Euclidian distance (IMED) between the feature attributes is used to measure the similarity among test image and the images in the database. Unlike Euclidian distance the IMED not only measures the intensity differences but also it considers the spatial relationship among the pixels into consideration. Hence it provides a better similarity measure between image pairs. Then the unknown image I is assigned to that class of image for which the IMED is minimum.

In a N class problem, let $T_k^{(i)}$ be the set of images in the database with $k=1, 2, 3, \dots, 14$ feature attributes and labeled to class i where $i=1, 2, 3, \dots, N$ and $T_k^{(i)} = [T_{k1}^{(i)} T_{k2}^{(i)} T_{k3}^{(i)} \dots T_{kt}^{(i)}]$.

Then the unknown image I is assigned to class N^* and defined as

$$N^* = \min_N \rho(I, T_k^{(i)}) \quad (12)$$

Where $\rho(I, T_k^{(i)})$ measures the distance between the feature attributes between the image I and $T_k^{(i)}$ is described in Eq. 13.

$$\rho(I, T_k^{(i)}) = IMED(I, T_k^{(i)}) \quad (13)$$

$$IMED^2(I, T_k^{(i)}) = \frac{1}{2\pi} \sum_{x,y=1}^{MN} \exp \left\{ - \left(\frac{|I_i - \{T_k^{(i)}\}_j|}{2} \right)^2 \right\} \times \left(I^x - \{T_k^{(i)}\}^x \right) \left(I^y - \{T_k^{(i)}\}^y \right) \quad (14)$$

where $|I_i - \{T_k^{(i)}\}|$ defines the pixel distance.

Table 5 provides the analysis of classification accuracy by using the NN classifier. It is observed that, the classification accuracy of the NN classifier using Combined Zernike moment invariant outperforms than others. By utilizing only 14 features the classifier achieves accuracy around 99%. Whereas, to achieve the identical accuracy 47 number of feature attributes based on geometric moment is needed. On the other hand 40 numbers of Legendre Moment based feature attributes are used to achieve an accuracy around 97% and 28 numbers of Zernike Moment based feature attributes are used to achieve an accuracy around 98%. From the above analysis, it is quite obvious that, selection of feature attributes using proposed method achieve an excellent tradeoff between the performance and computational time.

Table 5: Recognition accuracy using NN classifier

Feature Type	Feature order	Number of features	Accuracy (%)
Geometric Moment	12	47	99
Legendre Moment	11	40	97
Zernike moment	9	28	98
Combined Zernike moment invariant	6	14	99

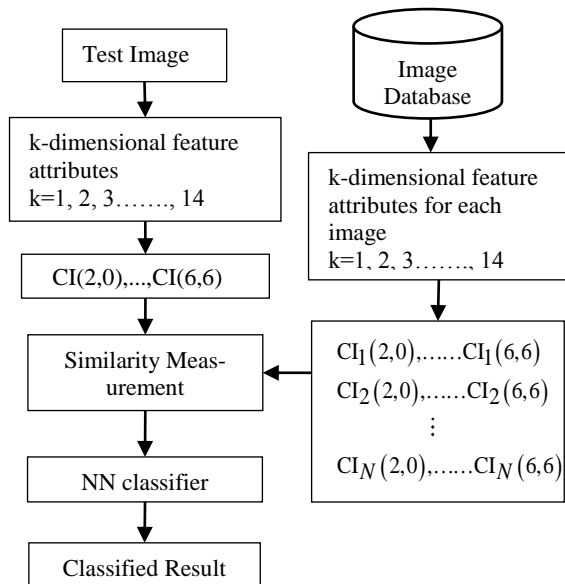


Fig. 6: Block diagram for object classification using Nearest Neighbor method

5. Conclusion

In this paper, a combined orthogonal Zernike moment based object recognition method is presented in which the extracted features are invariant to scale, rotation and transformation. This method extracts the feature that is best for object detection. Besides this, an efficient algorithm is proposed to select the optimum moment order for reconstructing the original part image from the geometrically distorted image. The NN classifier helps in recognizing the correct part. This part recognition methods is an efficient method recognizing parts in vision guided robotic part assembly environment.

References

- [1] Hu, M.K., (1962). Visual pattern recognition by moment invariants. IRE transactions on information theory, 8(2), pp.179-187.
- [2] A. Khotanzad and Y.H. Hong, (1990). Invariant image recognition by Zernike moments. IEEE Transactions on pattern analysis and machine intelligence, 12(5), pp.489-497.
- [3] A. Khotanzad and Y. H. Hong, (1990). Invariant image recognition by Zernike moments. IEEE Transactions on pattern analysis and machine intelligence, 12(5), pp.489-497.
- [4] J. Flusser and T. Suk, (1994). A moment-based approach to registration of images with affine geometric distortion. IEEE transactions on Geoscience and remote sensing, 32(2), pp.382-387.
- [5] L. Keyes and A. Winstanley, (2001). Using moment invariants for classifying shapes on large-scale maps. Computers, Environment and Urban Systems, 25(1), pp.119-130.
- [6] C.W. Chong, P. Raveendran and R. Mukundan, (2004). Translation and scale invariants of Legendre moments. Pattern recognition, 37(1), pp.119-129.
- [7] M. Mercimek, K. Gulez and T. V. Mumcu, (2005). Real object recognition using moment invariants. Sadhana, 30(6), pp.765-775.
- [8] J. Flusser, (2006). Moment invariants in image analysis. In proceedings of world academy of science, engineering and technology, 11(2), pp. 196-201.
- [9] K. M. Hosny, (2010). Robust template matching using orthogonal Legendre moment invariants. Journal of computer science, 6(10), p.1083.
- [10] Z. Yang and T. Fang, (2010). On the accuracy of image normalization by Zernike moments. Image and Vision computing, 28(3), pp.403-413.
- [11] B. Chen, H. Shu, H. Zhang, G. Coatrieux, L. Luo and J. L. Coatrieux, (2011). Combined invariants to similarity transformation and to blur using orthogonal Zernike moments. IEEE Transactions on Image Processing, 20(2), pp.345-360.